8-2019

Simulation of a Time-Varying Distributed Cathode in a Linear Format Crossed-Field Amplifier

Marcus Pearlman
Boise State University

Jim Browning
Boise State University

 doi: 10.1109/TPS.2019.2924376

Simulation of a Time-Varying Distributed Cathode in a Linear Format Crossed-Field Amplifier

Marcus Pearlman, *Member, IEEE* and Jim Browning, *Senior Member, IEEE*

***Abstract*— The effects of a temporally modulated, distributed cathode in a linear format crossed-field amplifier (CFA) are simulated in VSim and analyzed. A linear format, 150 MHz, low power (100 W), moderate gain (7 dB), meander line CFA is used as the basis for the simulation model. This paper describes simulations with different time-varying distributed cathodes in which electron injection is modulated at the RF frequency both in and out of phase with the RF input. At low RF input power the modulated electron injection dominates the operation. Injecting in phase with the RF input shows gain increases from 23 dB at 150 mA to 32 dB at 1 A for low cathode modulation power (<0.1 W). The CFA efficiency increased from 2-4% to 20-24% using the electron modulation. The simulation shows distinct cylindrically shaped electron bunches as opposed to spokes because of the synchronous injection. These results suggest that for high power magnetrons electron modulation could improve gain.**

***Index Terms*— Crossed-field amplifier (CFA), distributed beam, microwave vacuum electron devices**

I. Introduction

Microwave Vacuum Electron Devices (MVEDs) are often used for high power and high frequency applications over their solid state counterparts. There are many different types of MVEDs, but this work focuses on crossed-field amplifiers (CFAs). The advantages of CFAs over other MVED types is the high power (~10 MW peak, 10 kW average) with good bandwidth (10-15%) in a compact size [1], [2]. The disadvantages of CFAs are the low gain (typically <20 dB) and relatively high noise [1], [2]. Even with the low gain, the compact size, high power, and high bandwidth is desirable and CFAs are used for radar, electronic countermeasures, and particle accelerators. The disadvantages of CFAs limit use of the device for many applications and improving the gain and noise characteristics would make the CFA much more appealing, and these aspects are the ultimate goal of this research. Current CFAs generally use a cylindrical format, operate with a backward or forward wave, and use a secondary emitting cathode [1], [2]. One relatively unexplored area of research is the use of gated field emission arrays (GFEAs) [3], [4] to improve current injection control. GFEAs are much more efficient electron current sources than typical thermionic cathodes [2]-[5]. GFEAs have higher modulation frequency capability [5], [6] with results indicating frequency modulation ~10 GHz, and they have the advantage of easy spatial control as the emitters can be fabricated in addressable arrays. The precise control over the current can provide a method to study the noise mechanisms in the device. There has been research on the use of GFEAs in MVEDs [6], but in general, they have not been implemented in products due to emission current limitations and reliability constraints. There is very limited published work on GFEA reliability and lifetime testing.

The goal of this research is to demonstrate via simulation a linear format CFA which uses GFEAs as the electron source to spatially and temporally vary the injected electron current density in order to maximize efficiency, gain, and bandwidth and to minimize noise. Here, temporal indicates modulation of the electron injection versus time at the RF frequency while spatial modulation is used to mean that the electron injection varies as a function of location. Hence, electrons can be modulated in time but at different locations along the cathode. By tailoring the current injection throughout the tube, it may be possible to improve the mode locking mechanism and increase gain. A limiting factor to gain in CFAs is the inability to retain a lock on the main amplifying mode at higher RF powers [2], [7]. As the RF drive level becomes low compared to the output power, it loses control over the frequency of the RF output. In this region, the RF output is noisy and poorly defined [8].

This paper is the second of two papers [9] studying a low frequency (150 MHz), low power (100 W), linear format CFAs. In this paper, the results from modulating the cathode are presented compared to the first paper in which only uniform emission was studied, and these new results clearly shown that the modulation can improve CFA gain and efficiency offering a potentially new method of operation. First, the simulation model is presented with the description of the emission modulation, followed by the modulation results and an analysis of those results.

II. Simulation Model

The CFA simulated here is based on a design from Northeastern University [10], [11]. A more detailed description of the original device is given in the original work and in our previous paper [9], but a short summary is given here. The device is a linear format, injected beam, 150 MHz

Manuscript received January 2, 2019. This work was supported in part by the U.S. Air Force Office of Scientific Research under Grant FA9550-12-C-0066 and in part by the Electrical and Computer Engineering Department, Boise State University. The review of this paper was arranged by Senior Editor D. A. Shiffler. (Corresponding author: Jim Browning.) The authors are with the are the Electrical and Computer Engineering Department at Boise State University, Boise, ID 83725 USA (e-mail: marcuspearlman@boisestate.edu; jimbrowning@boisestate.edu;).

CFA which uses a meander microstrip slow wave circuit. The original circuit was 40 cm long and 25 cm and had a 1 cm pitch. With a retardation of R=33, the device was relatively short (6 slow wave wavelengths) and had relatively low gain (7 dB) [10], [11].

The simulation software used is VSim, which is a particle-in-cell code which solves for both the electromagnetic and electrostatic fields and for particle motion [12]. The simulation model is discussed in great detail in [9], but a short description is given here. Note that there are differences between the simulation and the original experiment, and these are described at the end of the section. Fig. 1 shows a 3D view of the injected beam configuration on a uniform grid. The injected beam configuration emits electrons from the cathode, whose potential is less negative than the sole so that electron loss to the sole is minimized when cycloiding down the tube. In the original model, the cathode potential was $V_{cathode}$ = 1050 V, the sole potential was V_{sole} = 1250 V, and the magnetic field was B = 5.2 mT. Electrons are emitted, cycloid down the tube, and interact with the RF signal on the meander line. The meander line is adjacent to the ground plane with dielectric in between, and it terminates into a 50 Ω coaxial output port identical to the input port. Figures showing the dimensions are described in section III.

The model uses both the electrostatic (Poisson's equation) and the electromagnetic (Yee finite difference time domain) solvers. The electrostatic and electromagnetic solvers use different boundary conditions. The boundary conditions for the electrostatic solver are shown in section III of [9]. They create the electric field between the cathode, sole, circuit, beam optic electrode, and end hats while keeping the simulation domain size minimized. The electromagnetic boundaries are all conducting boundaries except for the active ports, which absorbs waves at a specific phase velocity.

Four different main cathode types were tested in this work: 1) injected beam, 2) static distributed beam, 3) modulated distributed beam, and 4) modulated injected beam. The injected beam configuration was simulated [9] and validated against the experimental NU data in [10], [11]. The static distributed beam configurations were also studied in that work. This paper focuses on the modulated distributed cathode and compares all cathode types. The modulated injected beam uses the same location for injection as the injected beam case.

The distributed cathode spans the length of the tube, so it simultaneously acts as the sole. The distributed cathode must emit electrons at a potential less negative than the potential observed from incoming electrons to prevent electron loss to the cathode/sole electrode. Experimentally this would be achieved using hop funnels [13]-[15] or lateral emitters [16]. Simulating these devices along with the CFA physics would be computationally infeasible; therefore, an approximation was developed called the divergence free region. The emitters themselves are not modeled, and electrons are simply emitted from this region as if from a flat surface. The electrons are emitted normal to the surface with no energy spread or emission angle. While this approximation does not represent the emission from GFEAs in general, the effects on the overall device concept is believed minimal because of the nature of the electron hub in crossed-field devices in which electron kinetic energy is not critical. The divergence free region and its effects are explained in [9]. This region allows emission of electrons from within vacuum at a potential less negative than the sole and prevents any charge buildup at the emission site.

Two different modulated emission profiles were tested and are shown in Fig. 2. The first modulated cathode simulation used a sinusoidal profile, which is described in Eq. 1. J_e is the emission current density, J_p is the peak current density, ω is the angular frequency, β is the wave number associated with the retarded wave, and φ is the phase offset used to synchronize maximums in beam currents with minimums of the x-component of the electric field. $\varphi = \varphi_t - \varphi_x + \varphi_{90}$ where φ_t accounts for a time offset, φ_x shifts the sinusoid starting point to under the input coax, and φ_{90} shifts the maximum to be under the input coax. φ_{offset} ranges from 0 to π and is the controlled phase offset used to determine the optimum synchronization between the beam profile and the RF wave.

$$J_e(x,t) = J_p\,(1/2 + 1/2 \sin(\beta x - \omega t + \varphi + \varphi_{offset})) \qquad (1)$$

The second modulated emission profile is the square wave profile. Eq. 2 describes the current density J_{pulse} for one pulse of the function using Heaviside functions. To describe multiple pulses, each pulse would have to be defined explicitly for the entire simulation time. To simplify and reduce computation time, the sine wave function is used in conjunction with the max and ceil functions, shown in eq. 3. The function *max(a,b)* takes the maximum value a and b, *ceil(a)* rounds up to the nearest integer, and y_{Lp} is the y value corresponding with the desired pulse width L_p .

$$J_{pulse} = J_p \{ H(x + L_p/2 - x_{offset} - v_p t) - H(x + L_p/2 - x_{offset} - v_p t) \} \qquad (2)$$

$$J_e(x,t) = J_p \text{ x } ceil\,(max(y_{Lp}, \sin(\beta x - \omega t + \varphi + \varphi_{offset}) - y_{Lp})) \qquad (3)$$

These functions allow the use in the simulation of distributed, temporally-varying electron injection along the length of the device. The frequency and phase of the current injection along with the spatial length of the injection is varied to study the effects on CFA performance.

Two important diagnostics in the simulation are the gain and the signal to noise ratio (SNR). The SNR is measured by using the power spectral density (PSD) at the operating frequency. The SNR values presented here are not an indication of absolute SNR and can only be used for relative comparisons. The instantaneous input and output power are calculated by integrating the Poynting vector in space across the input and the output. The total input or output power are the average of this signal, but for lower RF powers, much of the power is actually noise. Therefore, the signal gain is determined using the power spectral density at the operating frequency. This approach calculates the output power, but only determines the RF input power at the input port. The modulated cathode itself will also dissipate power in the GFEA.

The power dissipated in the GFEA is not accounted for in the simulation and is estimated using the method in Calame et. al. for the resonant case [17]. The input signal is modeled as a

sinusoidal wave with a DC offset. The DC offset is set so that the sine wave can effectively turn on and off the current without requiring modulation of the full operational voltage. Hence, the DC offset is chosen to be just below the GFEA turn-on voltage to minimize the modulation voltage requirement. For our modeling, we have chosen to use the GFEAs fabricated by Gutierrez et. al. [4], [18], [19]. The capacitance of these structures was calculated by their group to be 1-5 nf/cm^2. The emission results demonstrated very high current density at low operating voltages making them ideal for our purposes to keep power consumption minimal. A simple model was created using the capacitance of an array covering the area of our distributed cathode design and using a DC offset voltage of 35V with the peak modulation voltage at 50 V. Therefore, the voltage on the GFEA gate swings from 20 – 50 V. Note that at 35V the GFEA does emit current, but the current magnitude is 2 orders of magnitude lower than the modeled peak current density of 10 mA/cm^2 at 50 V and is considered "off" for our calculations. Depending on the bandwidth needs, a resonant or a semi-resonant variant circuit could be used to drive the cathode. Also, an optically gated emitter circuit or optically stimulated emission could be used. Using the given cathode modulation drive signal for a simple sinusoidal resonant circuit, the estimated power consumed by the GFEAs [4], [18], [19] at 150 MHz is 0.1-1 W depending on the estimated capacitance for the array. If a square wave pulse is used, the power consumption would be substantially higher (~50 W). Hence, an attempt is made to account for GFEA power consumption by using simple models and then use that result to compare the effects on device gain.

Given the relatively low power of the device simulated, P_{out} = 100 W with J_{beam} = 100 mA/cm^2, the RF power needed to modulate the GFEA cathode is relatively high, 1% of P_{out} for $P_{fea} \approx 1$ W and results in a significantly lower gain. For higher power devices, P_{out} ~ 10 kW with J_{beam} >1 A/cm^2, the RF power needed to modulate the cathode is very conservatively estimated to be P_{fea} < 5 W which is < .05% of P_{out} which would provide a better comparison as the goal is to improve high power devices. To this end, two different gain calculations are shown for the modulated cathode using P_{fea} = 0.1 W and 1 W. The low power representation of gain is shown as an example of how the gain might appear for a higher power device (>10 kW).

There are a few notable differences between the simulation model and the actual experiment. To enhance the differences between different current distributions, the circuit was elongated by 50% (60 cm) in the simulation. Another difference is that the simulation uses a sole potential of V_{sole} = 1550 V to better compare the distributed cathode cases. Because most of the distributed cathode is located below the slow wave circuit, at the original parameters, most of the current would be collected on the slow wave circuit. The only way to optimize the gain of the device was to alter the anode-to-sole voltage and the magnetic field to ensure maximum gain for any configuration. All cathode types used this voltage for a meaningful comparison. The magnetic field and cathode voltage were optimized for each cathode configuration to maximize gain for a comparison. The distributed cathode configurations all used a magnetic field of B = 6.5 mT and emitted from a potential 200 V less negative than the sole. The injected beam cases use a magnetic field of B = 6.7 mT and an injected beam voltage of $V_{cathode}$ = 1150 V. In summary, the cathode length was increased to make it electrically long for improved gain; then for each cathode type, the operating parameters (magnetic field and voltage) were optimized to achieve maximum gain.

III. Simulation Results

A. Static Distributed Cathode Results

The prior work [9] suggested that there are two factors that contribute to gain when using a static cathode: 1) electron coupling distance and 2) electron trajectory. The electron coupling distance is the effective distance that the electron interacts with the slow wave circuit. Electrons injected farther down the tube have a shorter coupling distance; thus they give up less energy to the RF wave. The electron trajectory itself also determines how efficient the coupling is. Electrons trajectories too far from the circuit transfer energy inefficiently, and electron trajectories too close to the slow wave circuit transfer energy well but usually collect on the circuit before giving up all of the energy.

B. Modulated Cathode Characteristics

For brevity, only results from the square wave profile are presented here because they accurately demonstrate the same trends as the sine wave profile. For the reference case, the emitting cathode length is L_e = 30 cm; the pulse width is L_p = 1 cm; the RF input power is 1 W, and the total beam current is I_{beam} =150 mA. The first studies investigated the effects of the phase alignment between the modulated beam and the RF wave on the circuit. By adjusting the controlled phase offset, the electrons can be emitted in the accelerating or decelerating regions of the RF wave input on the circuit. The phase offset is swept from 0-2π rad, and the gain and SNR are shown in Fig. 3 as a function of the phase difference. The gain achieves a maximum of 14 dB when electrons are injected in phase with the decelerating region which corresponds with $\varphi_{offset} = \pi$ rad. When electrons are injected in the accelerating regions, the gain does not go to zero, but to 11 dB.

Typically, electrons in accelerating regions remove energy from the RF wave while electrons in decelerating regions give up their energy to the RF wave. The modulated current on the cathode actually drives the RF wave on the circuit, overpowering the injected RF signal. To investigate this phenomenon, the gain and the phase of the RF signal on the slow wave circuit is monitored. The phase and the gain are determined by the voltage along the length of the circuit. The voltage is measured by a psuedovoltage diagnostic between the meander line and the ground plane at various locations along the length of the of the slow wave circuit. The phase and the gain along the length of the circuit are shown in Fig. 4. The phase of the RF signal starts at 0 rad and shifts to approximately -0.9π rad, which is in phase with the modulated beam, after about 4 wavelengths (12 cm). The gain decreases until about 3 wavelengths and increases for the rest of the circuit as the RF phase is aligned with the modulated cathode phase. The gain in Fig. 4b is shown along with the theoretical gain predicted by Pierce theory for CFAs with unmodulated cathodes [20], [21]. As shown, the effect of electron

modulation is that optimal performance occurs when the electrons are in phase, but even out of phase, the modulation can dominate the RF input signal.

C. Cathode Comparison

Two studies were performed to compare the different cathode configurations versus RF input power and versus beam current. Fig. 5 shows the effects of the RF input power on the gain and the SNR for three cathode configurations: the modulated cathode square pulse profile, the injected beam, and the modulated injected beam. For the modulated cathode case, the gain (Fig. 5 (a)) was calculated using 0.1 W and 1 W of cathode modulation power. For the SNR in Fig. 5(b), the modulation power is not relevant. Fig. 6 shows the effects of beam current on the gain and SNR for the uniform distributed cathode and for the modulated cathode for the two cathode modulation powers (0.1 W and 1 W). The uniform distributed cathode used L_e = 20 cm, and the square pulse modulated cathode used L_e = 30 cm. The lengths were chosen such that space charge did not inhibit current and such that the cathode length was as short as possible. The modulated cathode has a higher current density, so it was spatially longer to reduce the space charge limits at high beam current. Note that it was not possible to simulate an injected beam case above 300 mA because of the high space charge at the injection site. The RF input power on the x-axis corresponds to the RF input power on the circuit and does not include the estimated GFEA power; however, the gain calculations do include the GFEA power.

As the RF input power is lowered, Fig. 5 shows that the gain for all the methods increases; the modulated cathode configurations have the highest gain. Note that lines on the plot go below $P_{rf} = 10^{-2}$ W. These lines are drawn to the 0W case which is plotted at $P_{rf} = 10^{-4}$ W (not shown) to use the log scale. At higher RF input powers (10 W), the gain of all methods converge to 7-8 dB. The SNR increases at higher input powers with the modulated cathode configurations 10-20 dB higher than the unmodulated. Hence, the cathode modulation improves gain and lowers the effective noise.

As the beam current is increased, Fig. 6 shows that the gain of each method increases. The uniform current case benefits the most from an increase in beam current, and actually surpasses the gain of the modulated cathode using the predicted cathode power of P_{fea} = 1 W; however in the case when the cathode modulation power is low (0.1 W) the gain is significantly larger at all beam currents. Hence, there is expected improvement for high power CFAs. The SNR is not shown for this case for brevity and because the SNR is relatively constant versus beam current. The SNR for the unmodulated cathode hovered around 50 dB at all currents, and the SNR for the unmodulated case increased from 28 dB to 31 dB at 200 mA and 800 mA, respectively. The calculated efficiency is shown in Fig. 6(b) to demonstrate the substantial increase in efficiency of the modulated case compared to the unmodulated uniform cathode. This increase was expected as the uniform distributed cathode current does not have time to interact with the RF signal over the circuit length. Note the decrease in efficiency in the modulated case with increasing beam current which appears to be related to space charge effects.

As a visual aid, the electron trajectories generated by the simulation are shown for each of the different cathode configurations with V_{as} = 1550V and I_{beam} = 150 mA. First, the electron trajectories for the square wave modulated distributed cathode profile are shown at different simulation times in Fig. 7. In this example, the electrons are in phase with the RF signal, and cylindrical electron bunches are observed. These cylindrical bunches move towards the circuit as the beam gives up potential energy to the wave. In the last plot (Fig. 7 (d)), the cylindrical bunch can be seen at the end of the device scraping off on the anode as electrons are collected. Fig. 8 shows the electron trajectories for four cathode configurations: injected beam, sine wave modulated distributed, uniform distributed (non-modulated), and modulated distributed beams. For each case two different RF input powers are used. The unmodulated cathode cases are shown in Figs. 8 (a, b, e, f) for P_{rf} = 0.5 mW and 10 W. As can be seen, the 0.5 W cases show very limited electron bunching; however the 10 W cases show significant bunching with actual cylindrical electron bunches observed in the higher power uniformly distributed beam case (Fig. 8 (f)). The modulated sinusoidal drive signal cases (Fig. 8(c,d)) show clear bunching effects at both 0 W and 1 W. These bunches are moving toward the anode and separating into discrete bunches. The modulated square profile distributed beam cases (Fig. 8(g,h)) are more striking. They show very clean cylindrical bunches that mode toward the anode. In the 10 W case, the last cylindrical bunch is nearly entirely collected on the anode demonstrating the improved efficiency of the modulation technique. Clearly, the electron modulation in phase has a significant impact on the electron trajectories, and since all electrons are in phase, very well-defined cylindrical spokes form.

IV. Analysis

A. Modulated Cathode Characteristics

The maximum gain in Fig. 3 occurs when the injected electrons are aligned with the decelerating regions of the electric field, $\varphi_{offset} = \pi$ rad. This matches theory very well; decelerating electrons give potential to the RF field on the circuit. Generally, electrons injected in the accelerating regions remove energy from the RF wave, but in Fig. 3 the gain remains above 10 dB at $\varphi_{offset} = 0$ rad. The moderate gain for unsynchronized beam profiles is due to the modulated electrons overpowering and driving the RF wave on the circuit. Fig. 4(a) shows the phase shift along the circuit matching the phase of the emission profile. Fig. 4(b) shows the gain along the circuit at first decreasing as the phase shifts and then increasing once the phase of the emission peak is aligned with the decelerating regions. When the emission profile is well aligned with RF wave, Fig. 4(a) shows little phase shift, and Fig. 4(b) shows the gain immediately increasing.

The main gain mechanism when using the modulated cathode is the beam modulation itself, and the RF input signal is the secondary mechanism. With no RF input power, the modulated distributed cathode output power is 43 W, and the

relative increase to the output power from changes in the input RF are rather small. Fig. 7 shows that adding an RF input on the circuit does contribute to the gain but becomes less significant at higher input powers. The RF circuit input does improve the operation efficiency; however the contribution to the RF output power is <2% of the total output power at the lower input powers, and this small efficiency improvement may not be enough to overcome the cost and complexity of implementing the timing between the RF signal on the circuit and the modulated cathode. This improvement might scale well with a higher power device, but it still needs study.

The cylindrical bunches observed in Fig. 7 are caused by the varying electron velocities in the cycloid trajectory. The cycloiding center point of the electron trajectories travels at the **ExB** velocity in the x-direction, but the electron velocity varies in the cycloid motion. The initial electron velocity after emission from the cathode is close to zero. The electrons accelerate in the y-direction because of the static electric field, and the magnetic field shifts the velocity in the x-direction where the maximum velocity in the x-direction occurs at the top of the cycloid. The magnetic field then drives the electrons back to the cathode, where the total velocity is close to zero near the cathode.

B. Cathode Comparison

The modulated cathode outperforms the unmodulated one in gain, SNR, and efficiency. The RF input power sweep shown in Fig. 5 demonstrates that the modulated cathodes outperform the unmodulated case for gain and SNR, even when accounting for the higher GFEA drive power. The unmodulated cathode extracts energy from the beam by modulating the beam through the interaction between the RF wave alone. At lower RF powers, the smaller electric fields reduce the energy extraction rate from the electron beam, resulting in lower maximum output power. In the modulated cathode, on the other hand, the pre-bunched beam drives the RF wave on the circuit, and any RF input signal modulation of the beam is a secondary, so the output power remains high even with low RF input powers on the circuit. With higher RF input powers on the circuit, all the methods tend to converge to the same output power as the amplifier saturates. The gain saturates as the electron beam becomes depleted as electrons collect on the slow wave circuit. The electron depletion is shown more clearly by Fig. 8(h). The cylindrical bunches move towards the SW circuit as they give up energy to the RF wave and get scraped off on the anode. The maximum efficiency of the device is around 35-40%, mainly limited by the highly cycloidal beam causing the electrons to be lost prematurely, before giving up all of their energy.

The modulated cathode beam performance demonstrates increasing gain vs. injection current, as shown in Fig. 6(a), up to 32 dB at 1 A for the low cathode modulation power (0.1 W). An increase in electron beam current decreases the beam impedance, which increases the gain and efficiency of the device according to Pierce theory [20], [21]. The uniform distributed cathode gain lies between the low and high power cathode modulation cases. The unmodulated cathode gain actually surpasses the modulated cathode when using the predicted cathode power of P_{fea}= 1 W and I_{beam} = 400 mA.

In Fig. 6 (b) the efficiency is much higher (20-24%) for the modulated case as electrons are injected in-phase; whereas the uniform cathode case is much lower (<4%) as electrons are injected out-of-phase. The efficiency actually decreases for the modulated case from 24% to 21%. Once again, the unexpected decrease in efficiency is caused by inefficient beam injection due to the increased space charge. The spreading of the electron bunches decreases efficiency faster than the efficiency improvement due to the inherent increase in beam current.

The SNR of the modulated cathode is consistently ≈ 20 dB greater than the unmodulated cathode. The SNR in the simulation is caused by simulation noise artifacts such macroparticles and grid approximation. Most of the noise in a real device is generated by the electron gun design and use of the thermionic cathode [22]. Because the noise is artificial and not representative of a real device, the SNR levels measured here are not meant to be taken absolutely. However, because each of the simulations are run with similar parameters, relative comparisons can be made.

V. CONCLUSION

There is a lack of published high power CFA designs, so a low power, linear format design was used for this study. In addition, while the simulated device was at 150 MHz and 100 W, the ultimate purpose of this research would be for higher frequency devices (0.9 – 10 GHz) and higher power (~1 MW) CFAs. The use of a modulated cathode was shown to inherently improve the performance of the device depending upon the calculated cathode modulation (GFEA drive) power. The improvements are limited by the GFEA drive power estimate, but because of the exponential I-V relationship of GFEAs, the GFEA drive power increases more slowly than the increasing device power including drive current. The modulated cathode improves the small signal gain and efficiency of the device, but in the saturation region for both higher beam and RF circuit input powers, the improvements over the unmodulated cathode are diminished. It is possible with higher beam powers than studied in this work, there may be no improvement using the modulated cathode. An apparent benefit of the modulated cathode at higher RF input powers is the lower SNR. This result implies that using the modulated cathode may reduce noise in CFAs. Current high-power CFAs have relatively low gain (< 20 dB) because of the necessity of a high RF drive power to retain lock on the main amplifying mode [2], [6]. Part of this limit is due to noise, and by reducing the noise, the modulated cathode may allow for even higher gain. Recall that the limit to gain in this model was the inability to inject more current and not due to the mode locking limit. In order to confirm this mode-locking hypothesis, the design of the model needs to be altered to overcome the space charge limit or a well-established high-power CFA design needs to be studied.

Implementing this device concept experimentally is a difficult one, mainly due to the frailty of the GFEA cathodes. While GFEAs have been modulated microwave frequencies [6], the frequency limitation is a major factor. It is not clear if modulation at sub-harmonics will provide similar performance improvements. Directly using the GFEAs in the interaction

region is most likely unfeasible due to the likelihood of damage from ion bombardment. Hop funnels provide a way to protect the GFEA cathode but would most likely limit the possible current density significantly. However, while current generation hop funnels are physically large [13], [14] (~1 mm spacing), these funnels can be much smaller (<0.1 mm) and could be used in smaller cathode structures to provide protection. The frequency modulation can be performed using either a delay line or active drive schemes such as solid-state transistors. The use of the periodic delay line provides both spatial and temporal modulation. An alternate implementation would be to use a hybrid option where GFEAs are used in conjunction with secondary emitting cathodes. The RF input and GFEA drive signals could be driven in-phase (synchronous) by a phase-lock-loop feedback configuration.

ACKNOWLEDGEMENT

The authors would like to thank TechX Corporation for the simulation support of Vsim including useful discussions with David Smithe, and we would like to thank Andy Yue for help in this paper preparation.

REFERENCES

[1] R. J. Barker, N. C. Luhmann, J. H. Booske, and G. S. Nusinovich, *Modern Microwave and Millimeter-Wave Power Electronics*. Hoboken, NJ, USA: Wiley, 2005.

[2] A. S. Gilmour, Jr., *Klystrons, Traveling Wave Tubes, Magnetrons, Crossed-Field Amplifiers, and Gyrotrons*. Norwood, MA, USA: Artech House, 2011.

[3] D. Temple, "Recent progress in field emitter array development for high performance applications," *Mater. Sci. Eng., R, Rep.*, vol. 24, no. 5, pp. 185–239, 1999.

[4] S. A. Guerrera and A. I. Akinwande, "High performance and reliable silicon field emission arrays enabled by silicon nanowire current limiters," in *IEDM Tech. Dig.*, Dec. 2015, pp. 33.1.1–33.1.4.

[5] C. A. Spindt, C. E. Holland, P. R. Schwoebel, and I. Brodie, "Field emitter- array development for microwave applications," in *IEDM Tech. Dig.*, Dec. 1995, pp. 389–392.

[6] D. R. Whaley, R. Duggal, C. M. Armstrong, C. L. Bellew, C. E. Holland, and C. A. Spindt, "100 W operation of a cold cathode TWT," *IEEE Electron Device Lett.*, vol. 56, no. 5, pp. 896–905, May 2009.

[7] J. F. Skowron, "The continuous-cathode (emitting-sole) crossed-field amplifier," *Proc. IEEE*, vol. 61, no. 3, pp. 330–356, Mar. 1973.

[8] W. C. Brown, "The platinotron: Amplitron and stabilotron," in *Crossed-Field Microwave Devices*, vol. 2, E. Okress, G. Mourier, J. Feinstein, and E. Kettlewell, Eds. London, U.K.: Academic, 1961, pp. 165–210.

[9] M. Pearlman and J. Browning, "Simulation of a Distributed Cathode in a Linear-Format Crossed-Field Amplifier," *IEEE Trans. Plasma Sci.*, vol. 46, no. 7, pp. 2497-2504, July, 2018.

[10] J. Browning, C. Chan, J. Z. Ye, and T. E. Ruden, "A low-frequency crossed-field amplifier for experimental investigations of electron-radio frequency wave interactions," *IEEE Trans. Plasma Sci.*, vol. 19, no. 4, pp. 598–606, Aug. 1991.

[11] J. Browning, C. Chan, J. Z. Ye, G. E. Dombrowski, and T. E. Ruden, "Electron plasma and wave measurements in a crossed-field amplifier and comparison with numerical simulation," *IEEE Trans. Electron Devices*, vol. 39, no. 10, pp. 2401–2407, Oct. 1992.

[12] *VSim Reference Manual*, TechX.

[13] B. H.W. Hendriks, G. G. P. van Gorkom, N. Lambert, and S. T. de Zwart, "Modes in electron-hopping transport over insulators sustained by secondary electron emission," *J. Phys. D: Appl. Phys.*, vol. 30, no. 8, pp. 1252–1264, Apr. 1997.

[14] M. Pearlman, T. Rowe, and J. Browning, "Simulation of electron hop funnel hysteresis," *IEEE Trans. Plasma Sci.*, vol. 41, no. 8, pp. 2291–2298, Aug. 2013.

[15] T. Rowe, M. Pearlman, and J. Browning, "Hysteresis in experimental I–V curves of electron hop funnels," *J. Vac. Sci. Technol. B, Microelectron. Process. Phenom.*, vol. 31, no. 4, p. 042204, 2013.

[16] J. Browning and J. Watrous, "Faceted magnetron concept using field emission cathodes," *J. Vac. Sci. Technol. B, Microelectron. Process. Phenom.*, vol. 29, no. 2, p. 02B109, 2011.

[17] J. P. Calame, H. F. Gray, and J. L. Shaw, "Analysis and design of microwave amplifiers employing field-emitter arrays," Journal of Applied Physics, vol. 73, no. 3, pp. 1485–1504, 1993.

[18] S. A. Guerrera and A. I. Akinwande, "Silicon field emitter arrays with current densities exceeding 100 a/cm2 at gate voltages below 75 v," IEEE Electron Device Letters, vol. 37, pp. 96–99, Jan 2016.

[19] S. A. Guerrera and A. I. Akinwande, "Nanofabrication of arrays of silicon field emitters with vertical silicon nanowire current limiters and self-aligned gates," Nanotechnology, vol. 27, no. 29, pp. 295–302, 2016.

[20] J. R. Pierce, "Traveling-wave tubes," *Bell Syst. Tech. J.*, vol. 29, no. 3, pp. 390–460, 1950.

[21] O. Buneman and G. Mourier, "Dynamic phenomena: Interaction of beams and circuits," in *Crossed-Field Microwave Devices*, vol. 1, E. Okress, G. Mourier, J. Feinstein, and E. Kettlewell, Eds. London, U.K.: Academic, 1961, pp. 367–438.

[22] R. M. Gilgenbach, Y.-Y. LAU, H. McDowell, K. L. Cartwright, and T. A. Spencer, "Crossed-field devices," in Modern Microwave and Millimeter-Wave Power Electronics, ch. 6, Wiley, 2005.

Marcus Pearlman (M'17) received the B.S. degree in electrical engineering from the University of Colorado at Boulder, Boulder, CO, USA, in 2005, and the M.S. and Ph.D. degrees from Boise State University, Boise, ID, USA, in 2012 and 2017, respectively. He is currently a research scientist at Boise State University. His current research interests include microwave vacuum electron devices and computational science.

Jim Browning (M'90–SM'08) received the B.S. degree and the M.S. degree in nuclear engineering from the Missouri School of Science and Technology, Rolla, MO, USA, in 1983 and 1985, respectively, and the Ph.D. degree from the University of Wisconsin–Madison, Madison, WI, USA, in 1988.

He was a Consultant in emission technology and a Senior Development Engineer with PixTech, Inc., Montpellier, France, and Micron Technology, Inc., Boise, ID, USA. He has been an Associate Professor with the Department of Electrical and Computer Engineering, Boise State University, Boise, ID, USA, since 2006. His current research interests include vacuum electron devices and cold atmospheric pressure plasma.

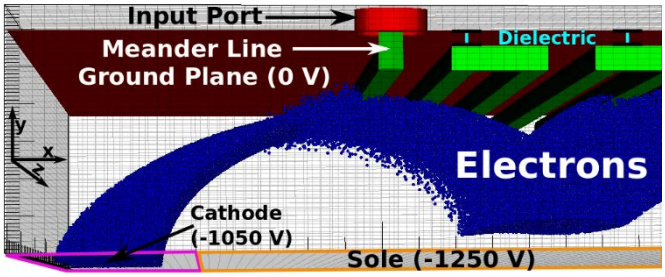

Fig. 1. Vsim 3D geometry with electrons. The RF wave is input on the upper y-edge of the domain, within the coaxial port. The RF wave travels within the dielectric region between the ground plane and the green meander line. Electrons are emitted from the cathode region, and cycloid right due to the crossed electric and magnetic fields. The electrons interact with the RF wave and give up their energy to amplify the RF wave.

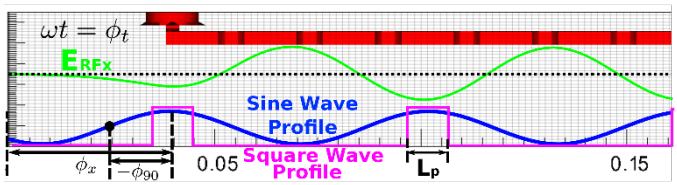

Fig. 2. The sine (blue) and square (magenta) wave electron emission profiles compared to the x-component of the RF field with φ_{offset} = 0 rad at $\omega t = \varphi_t$ .In this case the profile peaks are in the accelerating regions of the RF wave (out of phase).

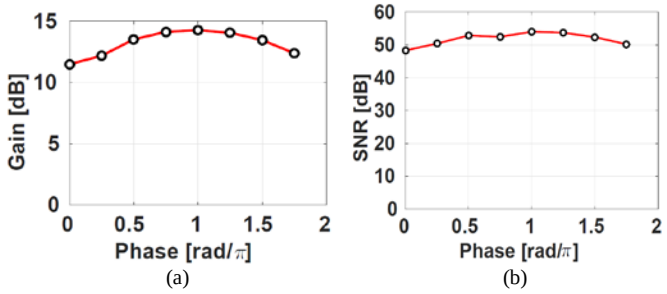

(a) (b)

Fig. 3. a) The gain and the corresponding (b) SNR vs. the phase difference between the beam profile and the RF wave for L_e = 30 cm, P_{rf} = 1 W, and I_{beam} = 150 mA.

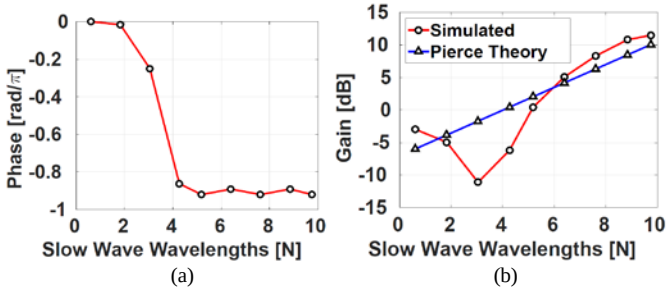

(a) (b)

Fig. 4. The (a) phase on the RF circuit and the (b) gain along the circuit for the square pulse profile with φ_{offset} = 0 rad, L_e = 30 cm, P_{rf} = 1 W, and I_{beam} = 150 mA.

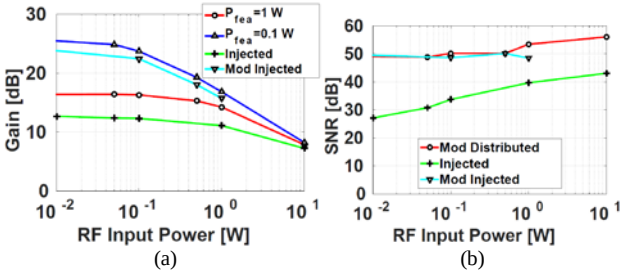

(a) (b)

Fig 5. (a) The gain and the corresponding (b) SNR vs. the RF input power on the circuit for both the modulated current and the injected beam with I_{beam} = 150 mA. The modulated cathode uses L_e = 30 cm. The RF input power on the x-axis does not include the modulated cathode power. In (a) both 0.1 W and 1 W cathode modulation powers are shown for the distributed cathode as well as the injected beam case and a modulated injected beam case.

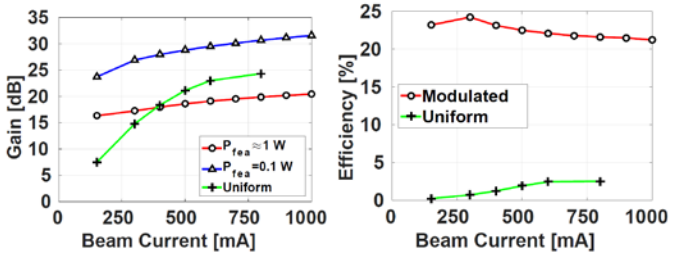

(a) (b)

Fig. 6. (a) The gain and the corresponding (b) efficiency vs. the beam current for both the modulated and uniform current distributions with the input P_{rf} = 0.1W. In (a), the modulated cathode power ≈ 1 W case includes actual estimated modulated cathode power (1 W at 150 mA and 2.5 W at 1000 mA), the 0.1 W modulated cathode power assumes a constant low power consumption. The modulated cathode uses L_e = 30 cm and the uniform current uses L_e = 20 cm.

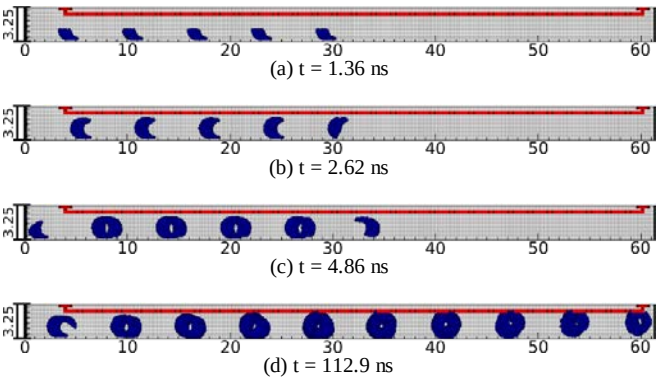

(a) t = 1.36 ns

(b) t = 2.62 ns

(c) t = 4.86 ns

(d) t = 112.9 ns

Fig. 7. Electron trajectories for the square pulse emission profile for V_{as} = 1550V and I_{beam} = 150 mA for different simulation times. Distance in centimeters.

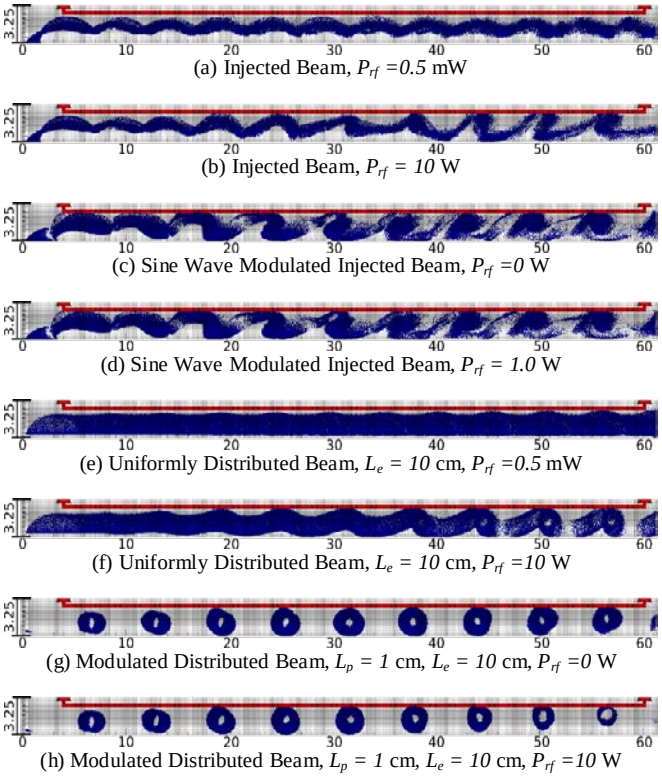

(a) Injected Beam, P_{rf} =*0.5* mW

(b) Injected Beam, P_{rf} = *10* W

(c) Sine Wave Modulated Injected Beam, P_{rf} =*0* W

(d) Sine Wave Modulated Injected Beam, P_{rf} = *1.0* W

(e) Uniformly Distributed Beam, L_e = *10* cm, P_{rf} =*0.5* mW

(f) Uniformly Distributed Beam, L_e = *10* cm, P_{rf} =*10* W

(g) Modulated Distributed Beam, L_p = *1* cm, L_e = *10* cm, P_{rf} =*0* W

(h) Modulated Distributed Beam, L_p = *1* cm, L_e = *10* cm, P_{rf} =*10* W

Fig. 8. Electron trajectories for various beam injection types (injected beam, sine wave modulated, distributed current unmodulated, and square profile modulated. Various RF input powers are shown for best visualization with V_{as} = 1550V and I_{beam} = 150 mA. Distance units in centimeters.